Influence of morphology on photoluminescence properties of methylammonium lead tribromide films

van de Riet, Irene; Fang, Hong-Hua; Adjokatse, Sampson; Kahmann, Simon; Loi, Maria A.

Published in:
Journal of Luminescence

DOI:
10.1016/j.jlumin.2020.117033

Publication date:
2020

Journal of Luminescence 220 (2020) 117033

Contents lists available at ScienceDirect

Journal of Luminescence

journal homepage: http://www.elsevier.com/locate/jlumin

Influence of morphology on photoluminescence properties of methylammonium lead tribromide films

Irene van de Riet, Hong-Hua Fang, Sampson Adjokatse, Simon Kahmann, Maria A. Loi *

Zernike Institute for Advanced Materials, University of Groningen, Nijenborgh 4, 9747, AG, Groningen, the Netherlands

A B S T R A C T

The morphology of hybrid perovskite thin films plays a crucial role for their photophysical properties. However, the underlying mechanisms are still unclear. To gain further insight into this phenomenon, methylammonium lead tribromide films of different morphology were investigated using photoluminescence spectroscopy. Photostability measurements demonstrate three mechanisms: (A) reversible degradation of the photoluminescence, depending positively on the grain-boundary density, which is presumably caused by photo-induced bromide vacancies, (B) enhancement of the photoluminescence intensity in the presence of oxygen and moisture and (C) destruction of the perovskite after several minutes of ultraviolet illumination with excitation power above 100 W/cm^2. Both the intensity and the lifetime of the photoluminescence were significantly smaller in films with micrometer-sized crystallites compared to granular films. This is ascribed to crystals being partially isolated in the former, causing smaller diffusion lengths, whereas the carriers in the granular films can diffuse from grain to grain resulting in higher photoluminescence lifetime and intensity.

1. Introduction

The study of hybrid perovskites flourished in the last decade and a multitude of articles showed their promising optoelectronic properties such as direct band gap, high absorption coefficients and long electron-hole diffusion lengths [1–5]. Besides the many advantages of hybrid perovskites, there are still obstacles on the way towards implementing them in real devices. An important issue is the dynamic behavior of the optical properties under illumination. Different studies of single crystal and polycrystalline thin films showed that both the intensity and the lifetime of the photoluminescence (PL) could be significantly improved by irradiation. This photo-induced effect was accounted for by the deactivation of defects that cause non-radiative charge recombination [6–8]. Furthermore, it has been shown that the presence of different environmental gases has also an important role on the enhancement of the PL intensity under illumination [9,10]. Excitation with ultraviolet light has a dual role, from one side it can boost the photoluminescence, from the other side in combination with oxygen and/or moisture can also result in degradation of the material [11–13]. Because of the interest in optoelectronic devices based on thin films, an important part of hybrid perovskite research is devoted to the study of polycrystalline thin films. Many studies report that photoluminescence properties of polycrystalline films and their performance in solar cells depend on the grain size of the material. This has been connected to grain boundaries, which are, naturally, more abundant for films containing smaller grains. Despite multiple attempts to unravel the influence of the boundaries, there is no agreement on their role on the physical properties of hybrid perovskites thin films [14–17]. Grain boundaries have been identified to be rich of charge traps, which have detrimental effects both for device performances and PL intensity [18,19]. Generally, the mechanism ascribed for the grain dependent variation of the optical properties are charge carrier diffusion followed by defect filling and ion migration, which is also indicated to be light induced [8,19–22].

While much work has been done for methylammonium lead triiodide and for the formamidinium variant, the properties of methylammonium lead tribromide ($CH_3NH_3PbBr_3$ or $MAPbBr_3$) thin films have not received enough attention. The investigations of the optical properties of this wide band-gap perovskite are actually key to solve the problem of the low efficiency displayed by this material in solar cells [23].

This work investigated the influence of the morphology of $MAPbBr_3$ thin films on their photoluminescence properties. The photostability of the light emission was mapped by performing measurements at various excitation densities and at different time scales. Three competing mechanisms were identified: (i) photo-induced trap state formation, (ii) passivation of trap states and (iii) decomposition of the perovskite. Their presence was linked to the film morphology. Furthermore, the different recombination mechanisms in the films were revealed through power dependent photoluminescence intensity and lifetime measurements.

* Corresponding author.
E-mail address: m.a.loi@rug.nl (M.A. Loi).

https://doi.org/10.1016/j.jlumin.2020.117033
Received 16 September 2019; Received in revised form 30 December 2019; Accepted 5 January 2020
Available online 7 January 2020

2. Results and discussion

2.1. Thin film morphology

The MAPbBr3 thin films that were investigated, were made with the use of spin coating. Three different recipes were followed, resulting in three different types of morphology. The spinning time, speed and acceleration were varied to create type I, II and III. Also, for type II and III, an anti-solvent was added before the end of the spinning process. The details of the recipes can be found in the experimental section.

X-ray diffraction measurements indicate that all three types of films are highly crystalline, but, as shown in the confocal laser scanning and scanning electron microscopy (SEM) images in Fig. 1, they form distinctly different morphologies.

Type I consists of crystallites (see Fig. 1a–c) clustered into groups. The surface of type II has a distinctive lamellar-like pattern, see Fig. 1d. Type III displays a similar lamellar-like pattern, see Fig. 1g. The different areas are composed of networks of shorter and longer assembly of crystallites. However, with respect to type II films the contrast between the darker and lighter regions is smaller.

In type I films the crystallites are well visible in both the confocal and the SEM microscopy image, see Fig. 1a–c. Comparison of the confocal microscopy images in Fig. 1e and h shows that the features on the surface of type II appear somewhat larger than those of type III. This corresponds well to the larger grain sizes for type II as indicated in the SEM images in Fig. 1f and i. The grains in Fig. 1i are less clear because of charging.

2.2. Dynamical behavior of the steady state PL

The photoluminescence properties of the thin films were investigated with a pulsed laser at 400 nm in air. The PL intensity was independent on the location of the excitation spot on the sample (see Fig. 3 and Supplementary Fig. 2). The measured PL intensity of the samples was unstable over time and both nature and extent of this instability depend on the morphology and laser intensity, see Fig. 2. With increasing laser power, the same general trend can be detected for all three morphology types.

At low excitation density, the PL intensity decreases rapidly and stabilizes at a low, but nonzero level (see upper curves). This decrement of PL occurs at a faster rate in type II and III samples compared to type I one. As the excitation intensity is increased, the PL intensity grows again after the initial decrement and is mostly followed by another drop in intensity (see middle curves). In general, the higher the laser power, the shorter the time of the initial intensity drop and the sooner the PL starts increasing again. Under highest excitation densities, the PL

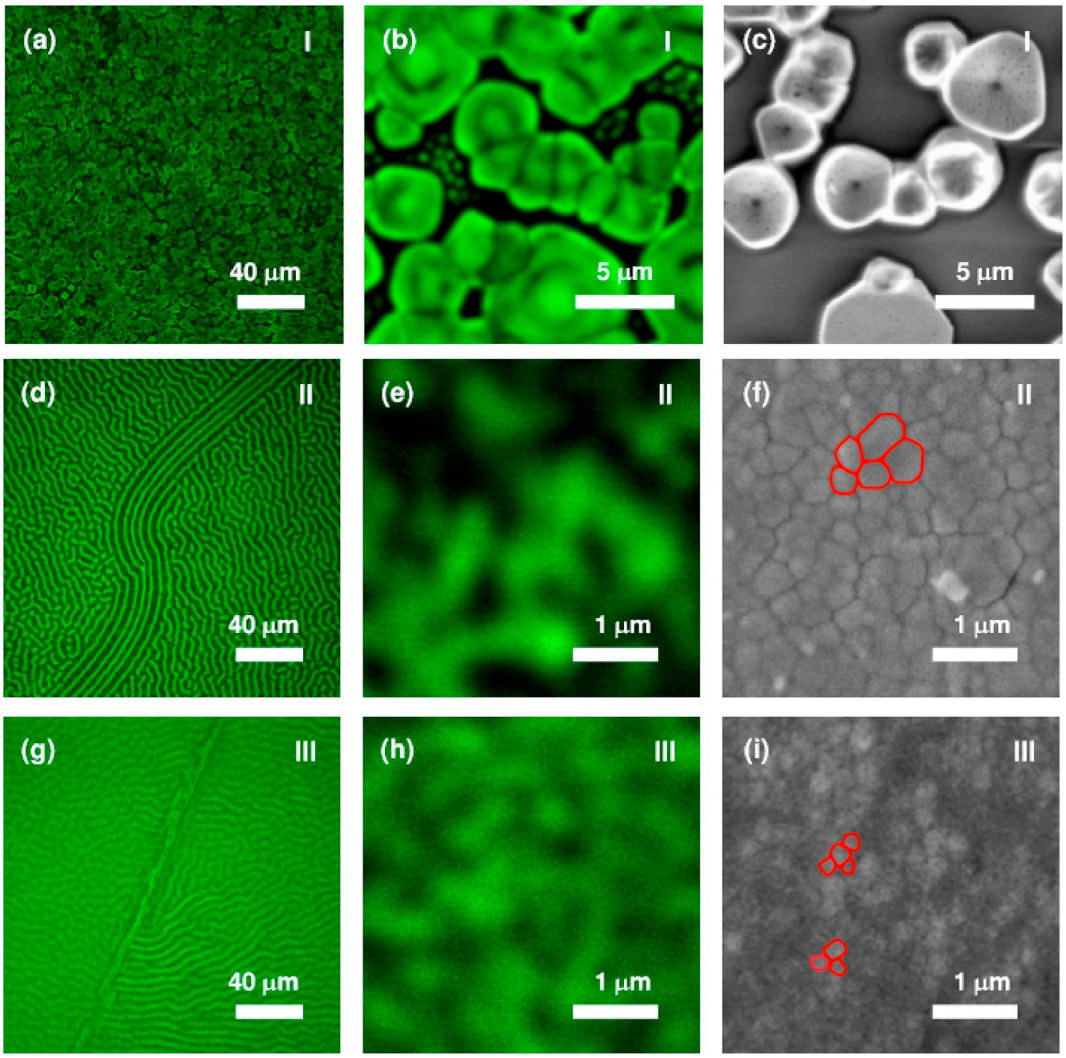

Fig. 1. Micrographs of the surfaces of the thin films of type I (a–c), II (d–f) and III (g–i) from top to bottom, respectively. Panels a, d, g and b, e, h, show the photoluminescence obtained from the surface with confocal laser scanning microscopy at two different length scales. The right panels (c, f, i), show the SEM micrographs at the same magnification as the higher resolution confocal images. For clarity, some grain boundaries in the SEM images in (f) and (i) are identified in red.

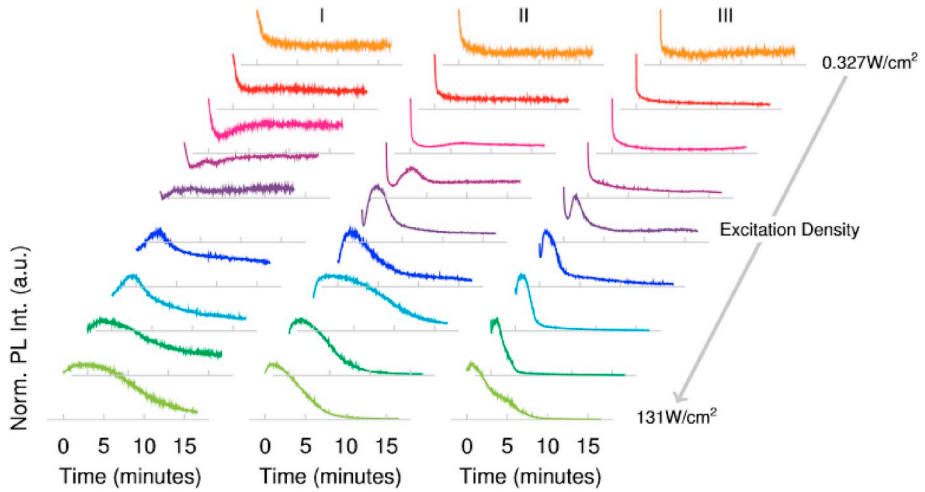

Fig. 2. Time sequences of the normalized photoluminescence intensity of type I, II and III films in air, at different excitation density (0.327, 0.654, 1.64, 3.27, 6.54, 16.4, 32.7, 65.4, 131 W/cm^2), while the films were continuously exposed to the laser. For each time sequence, a new spot on the film was excited. The time sequences are normalized to their maximum value.

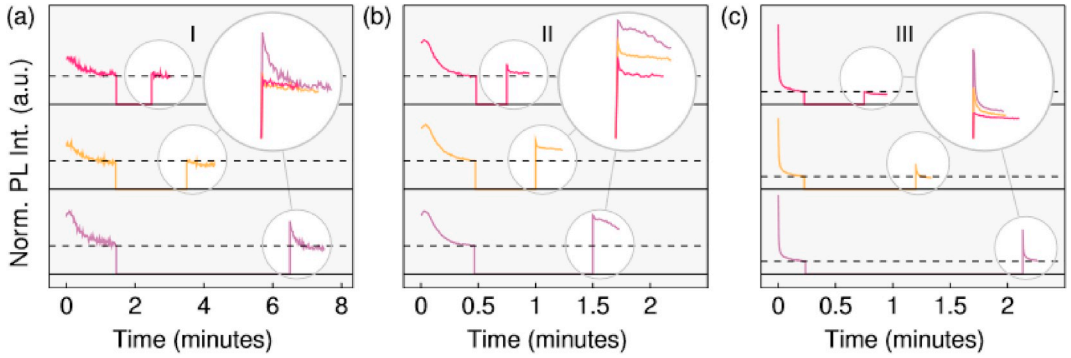

Fig. 3. (a–c) Time sequences of normalized photoluminescence intensity of type I, II and III under low intensity excitation. The films were continuously illuminated starting at t = 0, then stored in the dark and illuminated again. The dashed lines indicate the intensity at the end of the first illumination step. For each type, the measurement was performed three times with various duration of the time in the dark increasing from top to bottom. For comparison, the PL responses of the second illumination are plotted together in the upper right corner of each graph.

enhancement sets in instantly without prior reduction (see lower curves). It is important to notice that even in presence of large intensity variations, no spectral changes were observed upon illumination of the samples.

The alternation of increment and decrement of the PL intensity within one-time sequence shows that different mechanisms are competing with each other. Three different processes are identified. The first mechanism (A) causes a fast PL reduction, best visible under low excitation power. The second mechanism (B) causes enhancement of the photoluminescence at intermediate and higher excitation density. Finally, process (C) causes again degradation of the PL intensity, but different from (A), this degradation occurs on a longer time scale and at high excitation power. These three mechanisms will be discussed separately below.

2.2.1. *Photo-induced trap state formation*

Fig. 2 clearly shows how mechanism (A) is most dominant at low power during the first minutes of the time sequence. Under these conditions, (B) and (C) are not observed. In order to verify if (A) is reversible, the films were exposed to the laser until the PL intensity had significantly dropped and subsequently stored in the dark before again measuring the PL intensity. The results of the experiment are depicted in Fig. 3.

The initial exposure time and storage time was different for the three morphology types since also their response varied. The initial PL of type I degraded by more than 30% during the first 90 s and only recovered significantly after 5 min in the dark, see Fig. 3a. On the other hand, the initial photoluminescence intensity of type II and III degraded much faster. Within 30 s for type II and 15 s for type III, the PL intensity decreased by a factor 2 and 5, respectively, see Fig. 3b and c. It is important to note that the PL recovered more quickly for these films.

The decrease of the photoluminescence intensity suggests that on a time scale of seconds, the number of charge carriers that recombine non-radiatively increases. In other words, illumination of the samples with a 400 nm laser creates trap states. A likely mechanism for these trap states is the formation of bromide vacancies [20,24]. The most favorable ion to move in $MAPbBr_3$ is bromide, since halide anion vacancies show the lowest formation energies in calculations [25–27]. Luo et al. observed that bromide vacancies could be induced by applying a bias and could be moved throughout the $MAPbBr_3$ crystal. More importantly, they demonstrated that the bromide vacancies increase non-radiative recombination [24]. The mobility of the bromide vacancies and its negative effect on photoluminescence explains the reversible degradation mechanism. We note that the calculated activation energy for ion migration at grain boundaries is significantly smaller than in the bulk, and the positive influence of grain boundaries on ion migration was confirmed experimentally [16,19]. This explains why the effect of (A) is the strongest in the grain-boundary rich type III sample and the weakest

in the grain-boundary poor type I.

2.2.2. Passivation of trap states

The enhancement of the photoluminescence at intermediate and high excitation power indicates an increase of radiative recombination over trap-assisted recombination. We propose that this is due to the passivation of trap states, as observed in single crystal $MAPbBr_3$ [9]. Since the increase in photoluminescence was attributed to the interaction of the perovskite with oxygen and water [28], we investigated whether the same process is responsible for the PL enhancement in the films. To this end, time sequences at various laser power were carried out in nitrogen atmosphere. The results, see Fig. 4, indeed show no PL increase, proving the absence of trap passivation. This shows that analogous to single crystals, oxygen, moisture or a combination of both, induces curing of trap states in thin films.

The degradation at 0.20 and 0.98 W/cm^2 is very likely caused by mechanism (A), since the degradation at this low excitation density was found to be (partially) reversible in the previous experiment, see Fig. 3. Therefore, in the absence of a competing trap-curing mechanism, the mechanism (A) depends on the laser power. Also, these measurements confirm that this photo-induced trap state formation is the quickest in type III and the slowest in type I.

2.2.3. Decomposition

The third mechanism, (C), is observed after several minutes of intense illumination of 198 W/cm^2. To verify whether this degradation is reversible or not, the degraded samples were stored in the dark for several minutes and subsequently exposed to the laser again, see Fig. 5a. During the second illumination, the photoluminescence intensity of type I and III starts at a lower value than before the storage in the dark. This is because previously passivated trap states became active again, as similarly observed by other authors [9,29]. Both time sequences show that the intensity increases again during the second illumination, but does not exceed the prior level of intensity. The time sequence of type II shows that when the photoluminescence is almost completely quenched, the PL intensity remains at the same intensity level after the sample was stored in the dark. The results in Fig. 5a show that degradation upon high intensity exposure is irreversible by short time storage in darkness. Confocal images taken six days after the above described measurements, furthermore show that exposed areas do not heal on a longer time scale. Fig. 5b exemplarily shows the confocal image of type II samples, where the dark spots indicate where laser illumination was performed.

Since the measurements were conducted in air, it is likely that the permanent degradation is caused by the interaction with light and oxygen, moisture or both, as often proposed in literature [12,13,30]. The presence of O_2 or H_2O has been proposed, under illumination, to interact with ions in the sample and finally break up the perovskite structure [31]. This obviously, is a possible source of permanent degradation of the material, as observed.

2.3. Power dependent photoluminescence intensity and lifetime

Having demonstrated the profound impact of the morphology on the photostability of the thin films, we turn to the impact on the carrier dynamics. To this end, we studied the power dependent PL intensity and lifetime of the films. Given the intricate intensity changes discussed above, measuring the absolute PL of these samples is prone to mistakes. We thus designed a careful approach for these measurements, in which we attempt to record the immediate PL response to laser exposure by opening the laser beam during a sequence of single shot measurements. The average PL intensity and lifetime for three separate measurement points are given in Fig. 6a and b, respectively. The PL lifetime is given by the time in which the PL intensity drops to 1/e of its maximum.

When the films are illuminated by the laser, the charge carrier kinetics can be described with

$$\frac{dn}{dt} = G - k_1 n - k_2 n^2 - k_3 n^3, \tag{1}$$

where n is the charge carrier density, t is the time, G is the carrier generation rate, k_1 is the monomolecular recombination constant, k_2 is the bimolecular recombination constant and k_3 is the trimolecular (Auger) recombination constant [32]. Monomolecular recombination can be radiative when excitons recombine or non-radiative if charge carriers recombine via trap states [33–35]. The monomolecular constant is therefore the sum of the radiative and non-radiative constant, $k_1^{(r)}$ and $k_1^{(nr)}$, respectively. Bimolecular recombination is considered to be radiative and Auger recombination non-radiative [36]. The PL intensity is given by the carrier density multiplied by the quantum efficiency which is the ratio between radiative and total recombination [37].

$$I_{PL} = \frac{{k_1}^{(r)} + k_2 n}{{k_1}^{(nr)} + {k_1}^{(r)} + k_2 n + k_3 n^2} n. \tag{2}$$

The data points in Fig. 6a show two trends for all three morphology types. At low power the photoluminescence intensity depends more or less quadratically on the excitation density and at high power, a more linear relation is observed. On a logarithmic scale, this corresponds to a slope of around 2 and 1, respectively. The quadratic dependence of PL intensity on excitation density indicates three things: (i) $k_2 n \ll {k_1}^{(nr)}$, (ii) $k_3 n^2 \ll {k_1}^{(nr)}$ and (iii) radiative monomolecular recombination is negligible compared to bimolecular recombination: $k_2 n \gg {k_1}^{(r)}$, since these inequalities lead to the following equation

$$I_{PL} = \frac{k_2 n^2}{{k_1}^{(nr)}}. \tag{3}$$

Both (i) and (iii) are a direct consequence of the fact that n is low in this regime and $k_1 \gg k_1 n \gg k_1 n^2$ in $MAPbBr_3$ films [37]. The third outcome (iii) suggests that, as expected from the low binding energy, a negligible number of excitons is formed in the samples [38,39].

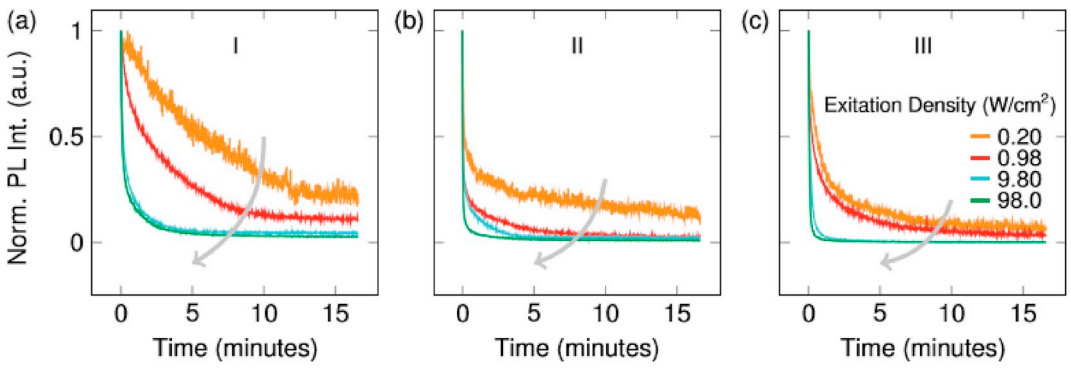

Fig. 4. (a–c) Time sequences of the normalized photoluminescence intensity of type I, II and III under nitrogen atmosphere, at different excitation density (0.20, 0.98, 9.80 and 98.0 W/cm^2). The higher the excitation density used, the faster the PL intensity drops. For each time sequence, a new spot on the film was excited.

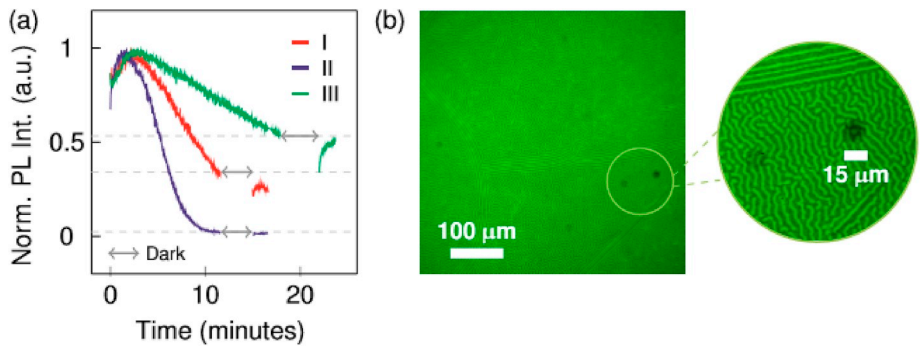

Fig. 5. (a) Time sequence of the normalized PL intensity under high excitation (196 W/cm^2). The intensity levels right before the films were stored in the dark, are indicated with gray dashed lines. (b) Confocal microscopy picture of a type II sample. The image was taken six days after PL measurements were performed on the sample. A magnification of the circled part displays the dark spots where previous illumination occurred.

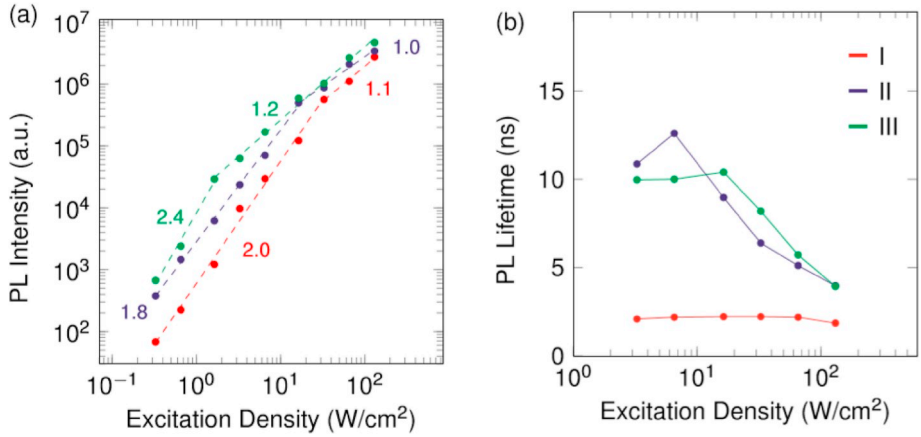

Fig. 6. PL intensity (a) and lifetime (b) of the thin films upon variation of the excitation intensity. Two straight dashed lines are fitted through each data set, their slopes are indicated in the figure.

The trend in the second regime indicates an almost linear dependence of the PL on the laser power, suggesting that non-radiative recombination becomes more dominant at higher excitation power. Both Auger recombination and mechanism (A) as well as mechanism (C) would give rise to this effect. It is unlikely that this is caused by Auger recombination, since the minimum charge carrier density that is needed for trimolecular recombination in $MAPbBr_3$ films, was found to be around 10^{18} cm^{-3} [40], which would correspond to an excitation density of around 300 W/cm^2 in our case. Since the PL intensity was established with measurements that were carried out within seconds after laser exposure (Supplementary Information (Supplementary Note 1), it is not likely that the monomolecular recombination is caused by mechanism (C), which works on a timescale of minutes. The decrease of radiative quantum efficiency is more likely caused by the photo-induced trap state formation, i.e. mechanism (A). The power dependent study carried out in nitrogen atmosphere (Fig. 4) shows that this process is stronger at high excitation power, which explains why the photoluminescence is quenched at this excitation. Additionally, the short time sequences at low power and measured in air (Fig. 3) and the time sequences measured in nitrogen atmosphere (Fig. 4) show that trap state formation is most strongly present in type III samples, followed by type II and is the weakest in type I. This clarifies why the quenching of the photoluminescence starts at lower laser power in type III, higher power in type II and starts at the highest laser power in type I.

Since more trap states were formed at high laser power, $k_1^{(nr)}$ increases with increasing n and the photoluminescence is therefore given by $I_{PL} = \frac{k_2 n^2}{k_1^{(nr)}(n)}$, where $k_1^{(nr)}$ is a function of n, resulting in a weaker, almost linear dependence of I_{PL} on n.

In Fig. 6b, all three types show the same general trend: the higher the laser power, the shorter the PL lifetime. This is again caused by the increased number of photo-induced trap states leading to more efficient non-radiative decays. The lifetime at the lowest excitation densities could not be established since the photoluminescence signal of these time resolved measurements were too weak. The lifetime of type II at 3.27 W/cm^2 and of type III at 3.27 and 6.54 W/cm^2 deviates from the general trend. This is probably caused by the weak and noisy photoluminescence signal at these excitation intensities, which gives rise to a less accurate lifetime estimation. A transient of each type of sample is given in Supplementary Fig. 4.

Over the entire range of excitation power, the PL intensity and the PL lifetime of type I is smaller than those of type II and III. The reason for this can be found in the difference of morphology. As Fig. 1a–c shows, the surface of type I consist of crystallites that are not always in contact with other crystallites but are isolated to a certain degree. Free charge carriers in isolated crystals cannot diffuse to other crystals. When the carriers move away from the center, they will get stuck at the crystal boundary. When, on the other hand, the crystallites touch each other, the interface functions as a grain boundary through which the carriers can eventually diffuse.

3. Conclusion

In this work, the influence of the morphology of methylammonium lead tribromide thin films on photoluminescence properties was studied. Three different types of films were investigated giving rise to three different mechanisms which affect their PL intensity. Photo-induced trap state formation (A) caused fast and partially reversible

degradation of the photoluminescence intensity at low and intermediate excitation density (below 16.4 W/cm^2) and is attributed to bromide migration. In addition, interaction of the perovskite with light and oxygen or moisture or a combination of the two caused passivation of trap states (B), which enhanced the photoluminescence intensity at intermediate and higher excitation density (from 1.6 W/cm^2). Finally, at high excitation density (198 W/cm^2), the photoluminescence intensity was irreversibly degraded due to decomposition of the material (C).

The photoluminescence intensity and the corresponding lifetime of type I sample was the smallest. This is attributed to the fact that the crystallites on the surface of type I are partially isolated. This gives rise to a shorter photoluminescence lifetime compared to what is measured for type II and III samples, where charge carriers can diffuse from grain to grain. It is interesting that the photoluminescence intensity is higher in type III than in type II. Which is attributed to the maze-like structure, evidenced by confocal microscopy.

4. Experimental section

4.1. Materials preparation

The $MAPbBr_3$ films were made by spin coating and were deposited on glass substrates. Materials were used as received. The solvents used for the solution were *N*,*N*′-dimethylformamide (DMF) (99.8%; Sigma-Aldrich) and dimethylsulfoxide (DMSO) (99.9%; Alfa Aesar), where the volumetric ratio of DMF:DMSO was 4:1. MABr and $PbBr_2$ (TCI Europe) were added such that their concentration in the solution was 1 M. Type I was created by spinning 30 s at 8000 rpm, with an acceleration of 4000 rpm/s. For type II, the substrate was spun for 30 s at 6000 rpm, with an acceleration of 6000 rpm/s and droplets of chlorobenzene were added as anti-solvent 10 s before the end. Type III was made by a two-step procedure: first the glass was spun for 5 s at 1000 rpm with an acceleration of 200 rpm/s and then for 15 s at 8000 rpm with an acceleration of 4000 rpm/s. Chlorobenzene was added 5 s before the end. Immediately after spinning, the samples were annealed at 100 °C for 10 min.

4.2. Confocal microscopy

Confocal laser scanning microscopy was performed with a set up based on an inverted Nikon Eclipse Ti microscope. All images were obtained using a single line continuous wave laser of wavelength 488 nm and an excitation power of 17 μW. The photoluminescence was recorded by the blue detector channel (515 ± 30 nm) and the green detector channel (590 ± 50 nm) and the images are a superposition of both channels.

4.3. Photoluminescence spectroscopy

The photoluminescence measurements were performed using the second harmonic (400 nm) of a mode-locked titanium-sapphire femtosecond laser (Mira 900, Coherent). The pulse repetition rate of the laser was adjusted with a pulse picker to 3.45 MHz. The illumination power density was adjusted by using neutral density filters. The excitation beam was spatially limited by an iris and focused with a 150 mm focal length lens. Emitted photons were collected with a lens and directed to a spectrograph. Steady-state spectra were collected using a Hamamatsu EM-CCD camera and time-resolved traces were recorded using a Hamamatsu streak camera in single sweep mode.

CRediT authorship contribution statement

Irene van de Riet: Methodology, Validation, Formal analysis, Investigation, Data curation, Writing - original draft, Visualization. **Hong-Hua Fang:** Conceptualization, Methodology, Writing - review & editing, Supervision. **Sampson Adjokatse:** Methodology, Validation, Investigation. **Simon Kahmann:** Writing - review & editing. **Maria A. Loi:** Conceptualization, Methodology, Resources, Writing - review & editing, Supervision, Funding acquisition.

Acknowledgements

S. Adjokatse acknowledges financial support from the NWO Graduate Programme, No. 022.005.006, and the Foundation for Fundamental Research on Matter (FOM), which is part of NWO, under the framework of the FOM Focus Group “Next Generation Organic Photovoltaics” for his doctoral studies. S.K. acknowledges the Deutsche Forschungsgemeinschaft (DFG) for a postdoctoral research fellowship (grant no. 408012143).

Appendix A. Supplementary data

Supplementary data to this article can be found online at https://doi.org/10.1016/j.jlumin.2020.117033.

References

[1] T. Baikie, Y. Fang, J.M. Kadro, M. Schreyer, F. Wei, S.G. Mhaisalkar, M. Graetzel, T. J. White, Synthesis and crystal chemistry of the hybrid perovskite (CH 3 NH 3) PbI 3 for solid-state sensitised solar cell applications, J. Mater. Chem. A 1 (18) (2013) 5628–5641.
[2] A.M.A. Leguy, P. Azarhoosh, M.I. Alonso, M. Compoy-Quiles, O.J. Weber, J. Yao, D. Bryant, M.T. Weller, J. Nelson, A. Walsh, et al., Experimental and theoretical optical properties of methylammonium lead halide perovskites, Nanoscale 8 (12) (2016) 6317–6327.
[3] S.D. Stranks, G.E. Eperon, G. Grancini, C. Menelaou, M.J.P. Alcocer, T. Leijtens, L. M. Herz, A. Petrozza, H.J. Snaith, Electron-hole diffusion lengths exceeding 1 micrometer in an organometal trihalide perovskite absorber, Science 342 (6156) (2013) 341–344.
[4] D. Shi, V. Adinolfi, R. Comin, M. Yan, E. Alarousu, A. Buin, Y. Chen, S. Hoogland, A. Rothenberger, K. Katsiev, et al., Low trap-state density and long carrier diffusion in organolead trihalide perovskite single crystals, Science 347 (6221) (2015) 519–522.
[5] G. Xing, N. Mathews, S. Sun, S.S. Lim, Y.M. Lam, M. Grätzel, S. Mhaisalkar, T. C. Sum, Long-range balanced electron-and hole-transport lengths in organic-inorganic CH3NH3PbI3, Science 342 (6156) (2013) 344–347.
[6] Y. Tian, M. Peter, E. Unger, M. Abdellah, K. Zheng, T. Pullerits, A. Yartsev, V. Sundström, I.G. Scheblykin, Mechanistic insights into perovskite photoluminescence enhancement: light curing with oxygen can boost yield thousandfold, Phys. Chem. Chem. Phys. 17 (38) (2015) 24978–24987.
[7] Y. Tian, A. Merdasa, E. Unger, M. Abdellah, K. Zheng, S. McKibbin, A. Mikkelsen, T. Pullerits, A. Yartsev, V. Sundström, et al., Enhanced organo-metal halide perovskite photoluminescence from nanosized defect-free crystallites and emitting sites, J. Phys. Chem. Lett. 6 (20) (2015) 4171–4177.
[8] H.H. Fang, F. Wang, S. Adjokatse, N. Zhao, M.A. Loi, Hong-Hua Fang, Photoluminescence enhancement in formamidinium lead iodide thin films, Adv. Funct. Mater. 26 (26) (2016) 4653–4659.
[9] H.H. Fang, S. Adjokatse, H. Wei, J. Yang, G.R. Blake, J. Huang, J. Even, M.A. Loi, Ultrahigh sensitivity of methylammonium lead tribromide perovskite single crystals to environmental gases, Sci. Adv. 2 (7) (2016), e1600534.
[10] J.F. Galisteo-López, M. Anaya, M.E. Calvo, H. Mîguez, Environmental effects on the photophysics of organic–inorganic halide perovskites, J. Phys. Chem. Lett. 6 (12) (2015) 2200–2205.
[11] A.M.A. Leguy, Y. Hu, M. Campoy-Quiles, M.I. Alonso, O. Weber, P. Azarhoosh, M. Van Schilfgaarde, M.T. Weller, T. Bein, J. Nelson, et al., Reversible hydration of CH3NH3PbI3 in films, single crystals, and solar cells, Chem. Mater. 27 (9) (2015) 3397–3407.
[12] R. Yang, L. Zhang, Y. Cao, Y. Miao, Y. Ke, Y. Wei, Q. Guo, Y. Wang, Z. Rong, N. Wang, et al., Inhomogeneous degradation in metal halide perovskites, Appl. Phys. Lett. 111 (7) (2017), 073302.
[13] Q. Wang, B. Chen, Y. Liu, Y. Deng, Y. Bai, Q. Dong, J. Huang, Scaling behavior of moisture-induced grain degradation in polycrystalline hybrid perovskite thin films, Energy Environ. Sci. 10 (2) (2017) 516–522.
[14] W.J. Yin, T. Shi, Y. Yan, Unique properties of halide perovskites as possible origins of the superior solar cell performance, Adv. Mater. 26 (27) (2014) 4653–4658.
[15] J.S. Yun, A. Ho-Baillie, S. Huang, Shujuan S.H. Woo, Y. Heo, J. Seidel, F. Huang, Y. B. Cheng, M.A. Green, Benefit of grain boundaries in organic–inorganic halide planar perovskite solar cells, J. Phys. Chem. 6 (5) (2015) 875–880.
[16] Z. Xiao, Y. Yuan, Y. Shao, Q. Wang, Q. Dong, C. Bi, P. Sharma, A. Gruverman, J. Huang, Giant switchable photovoltaic effect in organometal trihalide perovskite devices, Nat. Mater. 14 (2) (2015) 193.
[17] A. Sharenko, M.F. Toney, Relationships between lead halide perovskite thin-film fabrication, morphology, and performance in solar cells, J. Am. Chem. Soc. 138 (2) (2015) 463–470.
[18] S. Shao, M. Abdu-Aguye, L. Qiu, L.H. Lai, J. Liu, S. Adjokatse, J. Jahani, M. E. Kamminga, H. Gert, T.M.T. Palstra, et al., Elimination of the light soaking effect

and performance enhancement in perovskite solar cells using a fullerene derivative, Energy Environ. Sci. 9 (7) (2016) 2444–2452.
[19] S. Shao, M. Abdu-Aguye, T.S. Sherkar, H.H. Fang, S. Adjokatse, G. ten Brink, B. J. Kooi, L.J.A. Koster, M.A. Loi, The effect of the microstructure on trap-assisted recombination and light soaking phenomenon in hybrid perovskite solar cells, Adv. Funct. Mater. 26 (44) (2016) 8094–8102.
[20] S. Chen, X. Wen, R. Sheng, S. Huang, X. Deng, M.A. Green, A. Ho-Baillie, Mobile ion induced slow carrier dynamics in organic–inorganic perovskite CH3NH3PbBr3, ACS Appl. Mater. Interfaces 8 (8) (2016) 5351–5357.
[21] Y. Shao, Y. Fang, T. Li, Q. Wang, Q. Dong, Y. Deng, Y. Yuan, H. Wei, M. Wang, A. Gruverman, et al., Grain boundary dominated ion migration in polycrystalline organic–inorganic halide perovskite films, Energy Environ. Sci. 9 (5) (2016) 1752–1759.
[22] F. Panzer, C. Li, T. Meier, A. Köhler S. Huettner, Impact of structural dynamics on the optical properties of methylammonium lead iodide perovskites, Adv. EnergyACS Energy Lett. Mater. 7 (16) (2017) 1700286.
[23] N.K. Noel, B. Wenger, S.N. Habisreutinger, J.B. Patel, T. Crothers, Z. Wang, R. J. Nicholas, M.B. Johnston, L.M. Herz, H.J. Snaith, Highly crystalline methylammonium lead tribromide perovskite films for efficient photovoltaic devices, ACS Energy Lett 3 (6) (2018) 1233–1240.
[24] Y. Luo, P. Khoram, S. Brittman, Z. Zhu, B. Lai, S.P. Ong, E.C. Garnett, D.P. Fenning, Direct observation of halide migration and its effect on the photoluminescence of methylammonium lead bromide perovskite single crystals, Adv. Mater. 29 (43) (2017) 1703451.
[25] R.D. Shannon, Revised effective ionic radii and systematic studies of interatomic distances in halides and chalcogenides, Acta Crystallogr. A 32 (5) (1976) 751–767.
[26] A. Buin, R. Comin, J. Xu, A.H. Ip, E.H. Sargent, Halide-dependent electronic structure of organolead perovskite materials, Chem. Mater. 27 (12) (2015) 4405–4412.
[27] K. Domanski, B. Roose, T. Matsui, M. Saliba, S.H. Turren-Cruz, J.P. Correa-Baena, C.R. Carmona, G. Richardson, J.M. Foster, F. De Angelis, et al., Migration of cations induces reversible performance losses over day/night cycling in perovskite solar cells, Energy Environ. Sci. 10 (2) (2017) 604–613.
[28] A. Kojima, K. Teshima, Y. Shirai, T. Miyasaka, Organometal halide perovskites as visible-light sensitizers for photovoltaic cells, J. Am. Chem. Soc. 131 (17) (2009) 6050–6051.
[29] M. Anaya, J.F. Galisteo-López, M.E. Calvo, J.P. Espinós, H. Mìguez, Origin of light-Induced photophysical effects in organic metal halide perovskites in the presence of oxygen, J. Phys. Chem. Lett. 9 (14) (2018) 3891–3896.
[30] J.F. Galisteo-López, M. Anaya, M.E. Calvo, H. Mìguez, Environmental effects on the photophysics of organic–inorganic halide perovskites, J. Phys. Chem. Lett. 6 (12) (2015) 2200–2205.
[31] N. Ahn, K. Kwak, M.S. Jang, H. Yoon, B.Y. Lee, J.K. Lee, P.V. Pikhitsa, J. Byun, M. Choi, Trapped charge-driven degradation of perovskite solar cells, Nat. Commun. 7 (2016) 13422.
[32] G. Xing, B. Wu, X. Wu, M. Li, B. Du, Q. Wei, J. Guo, E.K.L. Yeow, T.C. Sum, W. Huang, Transcending the slow bimolecular recombination in lead-halide perovskites for electroluminescence, Nat. Commun. 8 (2017) 14558.
[33] S.D. Stranks, V.M. Burlakov, T. Leijtens, J.M. Ball, A. Goriely, H.J. Snaith, Recombination kinetics in organic-inorganic perovskites: excitons, free charge, and subgap states, Phys. Rev. Appl. 2 (3) (2014), 034007.
[34] J.M. Ball, A. Petrozza, Defects in perovskite-halides and their effects in solar cells, Nat. Energy 1 (11) (2016) 16149.
[35] M.B. Johnston, L.M. Herz, Hybrid perovskites for photovoltaics: charge-carrier recombination, diffusion, and radiative efficiencies, Acc. Chem. Res. 49 (1) (2015) 146–154.
[36] Y. Yang, M. Yang, Z. Li, R. Crisp, K. Zhu, M.C. Beard, Comparison of recombination dynamics in CH3NH3PbBr3 and CH3NH3PbI3 perovskite films: influence of exciton binding energy, J. Phys. Chem. Lett. 6 (23) (2015) 4688–4692.
[37] I. Pelant, J. Valenta, Luminescence Spectroscopy of Semiconductors, Oxford University Press, 2012.
[38] V. D'innocenzo, G. Grancini, M.J.P. Alcocer, A.R. S Kandada, S.D. Stranks, M. M. Lee, G. Lanzani, H.J. Snaith, A. Petrozza, Excitons versus free charges in organo-lead tri-halide perovskites, Nat. Commun. (2014) 3586.
[39] M. Saba, M. Cadelano, D. Marongiu, F. Chen, V. Sarritzu, N. Sestu, C. Figus, M. Aresti, R. Piras, A.G. Lehmann, et al., Correlated electron–hole plasma in organometal perovskites, Nat. Commun. 5 (2014) 5049.
[40] J.M. Richter, M. Abdi-Jalebi, A. Sadhanala, M. Tabachnyk, J.P.H. Rivett, L. M. Pazos-Outòn, K.C. Gödel, M. Price, F. Deschler, R.H. Friend, Enhancing photoluminescence yields in lead halide perovskites by photon recycling and light out-coupling, Nat. Commun. 7 (2016) 13941.